Check for updates

This article can be cited before page numbers have been issued, to do this please use: M. Queralt-Martín, D. A. Perini and A. Alcaraz, *Phys. Chem. Chem. Phys.*, 2020, DOI: 10.1039/D0CP04486E.

Physical Chemistry Chemical Physics Accepted Manuscript

Specific adsorption of trivalent cations in biological nanopores determines conductance dynamics and reverses ionic selectivity

María Queralt-Martín[*], D. Aurora Perini and Antonio Alcaraz

Laboratory of Molecular Biophysics, Department of Physics, Universitat Jaume I, 12071 Castellón, Spain

*Corresponding author: mqueralt@uji.es

Keywords. Selectivity Inversion; Current Modulation; Ion Channel; Equilibrium and Non-equilibrium Fluctuations; Charge Regulation;

Abstract

Adsorption processes are central to ionic transport in industrial and biological membrane systems. Multivalent cations modulate the conductive properties of nanofluidic devices through interactions with charged surfaces that depend principally on the ion charge number. Considering that ion channels are specialized valves that demand a sharp specificity in ion discrimination, we investigate the adsorption dynamics of trace amounts of different salts of trivalent cations in biological nanopores. We consider here OmpF from *Escherichia coli*, an archetypical protein nanopore, to probe the specificity of biological nanopores to multivalent cations. We systematically compare the effect of three trivalent electrolytes on OmpF current-voltage relationships and characterize the degree of rectification induced by each ion. We also analyze the open channel current noise to determine the existence of equilibrium/non-equilibrium mechanisms of ion adsorption and evaluate the extent of charge inversion through selectivity measurements. We show that the interaction of trivalent electrolytes with biological nanopores occurs *via* ion-specific adsorption yielding differential modulation of ion conduction and selectivity inversion. We also demonstrate the existence of non-equilibrium fluctuations likely related to ion-dependent

trapping-detrapping processes. Our study provides fundamental information relevant to different biological and electrochemical systems where transport phenomena involve ion adsorption in charged surfaces under nanoscale confinement.

Author's email addresses:

María Queralt-Martín: mqueralt@uji.es

D. Aurora Perini: perini@uji.es

Antoni Alcaraz: alcaraza@uji.es

1. Introduction

Transport of ionic species through micro- and nanofluidic devices is critically governed by surface charge as shown in a variety of engineered systems and biological ion channels [1–7] . Among other processes, adsorption processes play a fundamental role on industrial membrane systems both changing the energy consumption and the ion exchange capacity [8,9]. In biomembranes, adsorbed and desorbed ions can critically alter the cell signaling by means of different mechanisms, among them modifying the membrane charge [10] or the protein function [4,11]. In particular, divalent and trivalent cations have a strong tendency to accumulate near charged regions of ion channels and nanopores yielding a change in the effective pore charge that may alter both the conductance (Ohmic versus rectifying pores) and ionic selectivity (cation versus anion preference) [3,12–18].

For our study, we consider a biological nanopore, OmpF from *Escherichia coli*, a protein channel that forms trimeric identical and independent pores when inserted in planar lipid bilayers [19,20]. OmpF has been considered a good representative of the so-called "mesoscopic pores": the channel eyelet is too wide to yield ion-specificity (contrary to K^+ or Na^+ channels) but the channel walls

are still close enough to regulate electrostatically the transport of small inorganic ions (K^+, Na^+, Cl^-, etc) [21–26] and also show effects of nanoscale confinement like access resistance [5,27].

The understanding of ionic permeation through nanometer-sized pores is challenging because both the molecular nature of the fluid and the channel itself become important. Biological ion channels allow studying structure-function correlations at atomic detail, pushing to its limits the conventional description of transport phenomena in membrane systems [1,27] and paving the way for the design of nanofluidic devices for a variety of technological applications such as energy conversion, biosensing, desalination or molecular separation among many others [28–35]. In previous studies, we showed that, when added in trace amounts, La^{3+} cations (La) have a decisive impact on the OmpF channel activity reducing the open channel conductance for positive but not for negative applied voltages [36,37]. Similar features have been extensively reported either in other channels [38–42] and synthetic nanopores [3,16,18,43,44]. Here we extend the study to other multivalent cations such hexaamminecobalt^{3+} ($[Co(NH_3)_6]^{3+}$) and spermidine^{3+} (1,4-Butanediamine, N-(3-aminopropyl)-) that show contrasting conducting features compared to those of La. Hexaamminecobalt^{3+} (HexCo) is a small molecule that shares charge with La and has been shown to block other bacterial outer membrane proteins like the efflux pump TolC [45]. Spermidine^{3+} (SPD) is a linear molecule carrying amine functional groups that confer a trivalent positive charge to the molecule. SPD is an endogenous molecule of *Escherichia coli* and has been shown to reduce antibiotic flux through OmpF, among other effects [46].

In recent studies with synthetic nanopores involving salts of monovalent and multivalent cations it has been shown that it is the valence of the ion rather than the particular ion considered what determines the nanopore conductive properties [18]. Although some specific effects have already been reported in abiotic nanopores [7,47], well-defined specificity between ions of the same valence

is essential in a more biological context. For instance, electrophysiological recordings of the antibiotic peptide gramicidin A showed strong specific interactions between trivalent cations and charged lipid bilayers that may even locally reverse the membrane charge [10].

To probe the degree of specificity of biological nanopores to trivalent cations, we compare the effect of trace amounts of La, HexCo and SPD on OmpF conductive properties, i.e. channel current and selectivity. We examine the current-voltage relationship of the channel and characterize the rectification induced by La, HexCo and SPD with the parameters typical for semiconductor n/p diodes. The novelty of the present work compared to previous studies, which focused mainly on the analysis of average channel currents, lays on the examination of the channel current noise properties (amplitude and frequency of current oscillations) through the calculation of the power spectral density (PSD) of the signal. By analyzing how PSD depends on the channel average current we show that the conductive properties of the bacterial channel OmpF can be modulated both by equilibrium and non-equilibrium mechanisms. On view of that, we extend our investigation to probe how these mechanisms reverse the ionic selectivity of the biological nanopore.

Identifying the sources of noise in nanometer-sized pores goes beyond the academic understanding of ion conduction at the nanoscale, but it could be useful in bioanalytical and large-scale technological application by helping to reduce the signal-to-noise ratio that determines the time resolution of experimental set-ups [48,49]. By combining this noise analysis with the study of current-voltage curves and selectivity inversion, we provide fundamental information on the specific interaction of multivalent ions with biological nanopores that should be relevant to other contexts such as synthetic nanopores and solid-state membranes [1,2,47].

2. Experimental

2.1. Materials

Diphytanoyl phosphatidylcholine (DPhPC) in chloroform was purchased from Avanti Polar Lipids (Alabaster, AL). The trivalent cations La, HexCo and SPD were purchased from Panreac (Lanthanum(III) chloride 7-hydrate, #122848) and Sigma (Hexaamminecobalt(III) chloride, #481521; Spermidine trihydrochloride, #S2501).

2.2. Membrane formation and channel insertion

Isolation and lab handling of OmpF channels was analogous to the method described elsewhere [12,21,22]. Wild-type OmpF, kindly provided by Dr. S. M. Bezrukov (NIH, Bethesda, USA), was isolated and purified from an *E. coli* culture. Planar membranes were formed by using a solvent-free modified Montal-Mueller technique [50,51]. In brief, lipid was prepared by dissolving DPhPC in pentane at 5 mg/ml after chloroform evaporation. Aliquots of 10-20 μl of lipid in pentane were added on top of each salt solution in two 1.6-ml compartments (so-called *cis* and *trans*) of a Teflon chamber. The two compartments were separated by a 15-mm-thick Teflon film with a 70-100-μm diameter orifice where the bilayer formed. The orifice was pre-treated with a 1% solution of hexadecane in pentane. After pentane evaporation, the level of solutions in each compartment was raised above the hole so the planar bilayer could form by apposition of the two monolayers. Spontaneous channel insertion was achieved by adding ~0.1 μL of OmpF at 1 ng/μL in 0.1 M KCl and 1% (v/v) OctylPOE (Alexis, Switzerland) to the *cis* compartment. It is well stablished that this protocol yields a channel insertion almost always (>95%) in the same orientation [21,22,37,52].

2.3. Electrical measurements

An electric potential was applied using Ag/AgCl electrodes in 2 M KCl, 1.5% agarose bridges assembled within standard 250 µl pipette tips. The working electrode was placed in the side of protein addition (the *cis* side of the membrane chamber) and thus the potential was defined as positive when it was higher on the *cis* side, whereas the *trans* side was set to ground. An Axopatch 200B amplifier (Molecular Devices, Sunnyvale, CA) in the voltage-clamp mode was used to measure the current and to apply potentials. Data were filtered by an integrated low pass 8-pole Bessel filter at 10 kHz, saved with a sampling frequency of 50 kHz and analyzed using pClamp 10.7 software (Molecular Devices, Sunnyvale, CA). The chamber and the head stage were isolated from external noise sources with a double metal screen (Amuneal Manufacturing Corp., Philadelphia, PA). The described set-up can resolve currents of the order of picoamperes with a time resolution below the millisecond.

Current measurements were performed with 100 mM KCl symmetrical solutions, while selectivity experiments were performed in a concentration gradient of 0.1 M / 1 M KCl or 1 M / 0.1 M KCl. In all experiments the pH was kept at pH 6 and no buffer was used to avoid interference with trivalent cations. The pH was adjusted by adding HCl or KOH and controlled during the experiments with a GLP22 pH meter (Crison). To assure reproducibility, single-channel conductance experiments were repeated a minimum of 3 times and selectivity experiments, which were performed in membranes with multiple channels inserted, were repeated at least 2 times. Millimolar concentrations of La, HexCo and SPD were added symmetrically at both sides of the membrane through addition of appropriated amounts of a 200 mM stock solution. After addition, solution at each side was homogenized with a syringe to assure proper mixing.

Selectivity was assessed by measuring the reversal potential (RP), which is the applied voltage needed to cancel the current measured when a salt concentration gradient is imposed in the system.

6

If the channel is neutral, RP equals zero, while it becomes nonzero when the channel is selective to anions or cations. When the concentration gradient is 0.1 M *cis* / 1 M *trans*, a positive RP corresponds to a cation selective channels; with the opposite gradient (1 M *cis* / 0.1 M *trans*), is a negative RP that indicates cationic selectivity. All RP values were corrected by the liquid junction potential from Henderson's equation[12] to eliminate the contribution of the electrode's agarose bridges.

2.3. Fitting of experimental data

To evaluate the diode-like characteristics of the current-voltage curves, an equation typical of semiconductor p/n diodes was used [53]. The voltage-dependence of the diode current I_d can be written as [10]:

$$I_d \propto \left[\exp\left(\frac{-eV}{nk_bT} \right) - 1 \right],\qquad(1)$$

where e, k_B and T have their standard meanings of electrical charge, Boltzmann constant and temperature, and n is an ideality factor that typically ranges between 1 and 2 for semiconductor diodes [53]. The fitting was performed simultaneously (using a unique value for n) for the three sets of control values presented in the manuscript (black circles in Figs. 2A-C) given that these data were obtained in the same conditions (100 mM KCl pH 6 before the addition of blocker) and the observed variability is inherent of single-channel experiments. Then, independent fittings were performed for 15 mM La, HexCo, and SPD.

2.4. Analysis of current fluctuations

The power spectral density (PSD) of current fluctuations was obtained directly from the measured current traces with the pClamp 10 software (Molecular Devices, LLC.). The PSD generates a frequency-domain representation of the time-domain data and provides a rich source of information about the underlying physical mechanisms that generate current fluctuations. The PSD reveals the power levels of the different frequency components present in the signal, allowing the identification of physical mechanisms that many times is difficult to obtain directly from current measurements [54]. PSD was measured by calculating the Fast Fourier Transform from the digitized signal after application of a 1 kHz 8-pole Bessel lowpass digital filter. The PSD spectral resolution used was 0.76-1.53 Hz and, for each signal, the available spectral segments were averaged.

The increase of the PSD amplitude as the square of the average current is a signature of conductance fluctuations. The PSD is the Fourier transform of the time-dependent autocorrelation function of the current $i(\tau) = <I(t) \cdot I(t+\tau)> - <I>^2$, so that $PSD \propto I^2 <\Delta I^2>/<I>^2$ and PSD/I^2 will be constant whenever $<\Delta I^2>/<I>^2 = $ constant [55,56]. Conductance fluctuations in an ion channel can be attributed to the pore itself or to the number of charge carriers. For fluctuations in the pore geometry or in the number of charge carriers when they are independent (so $I = Ni$, $<I> = N<i>$ and $<\Delta I^2> = N<\Delta i^2>$), the equality $<\Delta I^2>/<I>^2 = $ constant is fulfilled [55–61].

3. Results and discussion

3.1. Differential modulation of OmpF current-voltage characteristics by trivalent cations

Ion channel reconstitution into planar synthetic membranes allows the study of conductance of biological nanopores at the single-protein level. Fig. 1 displays the current traces of an OmpF single channel in a symmetric 100 mM KCl electrolyte at ±50 mV before and after the addition of

millimolar concentrations (10 mM) of chloride salts of La, HexCo or SPD. Before trivalent cation addition (Control), OmpF current is stable with a conductance of 0.7 ± 0.1 nS. OmpF is a trimeric channel, with three identical subunits that function independently in their open state [21]. At high voltages, monomers can close yielding to a ~1/3 current drop [62], what is called *channel gating*. Our experiments are carried at low enough voltages to avoid monomer closing. When salts of La, HexCo or SPD are added symmetrically to the system, a decrease of channel conductance is found, either maintaining similar conductive levels in both polarities (HexCo and SPD) or inducing asymmetric conduction (La). These findings are at odds with the fact that millimolar concentrations of salts of multivalent cations increase the ionic conductivity of the initial KCl solution. Therefore, there must be some kind of specific interaction between the OmpF channel and trace amounts of trivalent cations that hinders the ion transport of the supporting electrolyte (KCl in the present case). In no case the channel is completely blocked, indicating that the trivalent cations either act on only one or two of the channel monomers or they do not completely block the monomer current.
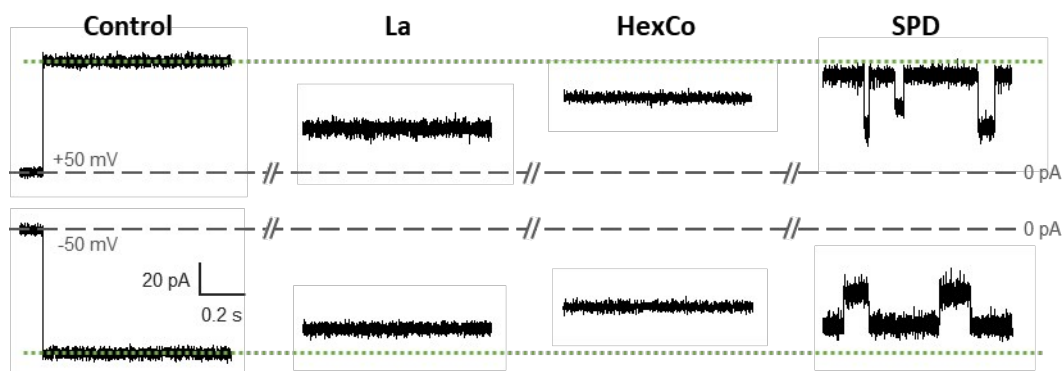

Figure 1. Symmetric addition of trivalent cations has a variable effect on OmpF single-channel current. Unitary current traces of a single OmpF channel inserted in a DPhPC membrane in 100 mM KCl salt solution at pH 6 before (Control) and after the addition of 10 mM lanthanum (La), hexaamminecobalt (HexCo) or spermidine (SPD) salts at both sides of the membrane cell. Current records were digitally filtered at 1 kHz using a low-pass Bessel (8-pole) filter.

While the three explored ions reduce the open channel current more or less asymmetrically, SPD also promotes the voltage-induced channel closure, as previously reported [63]. Note that the modulation of the open channel conductance is essentially different from the voltage gating [36], observed in control traces at much higher voltages [19,62,64]. Interestingly, only SPD has an effect in relation to voltage-induced gating, which occurs indistinguishably at both voltage polarities. Actually, the gating is so intense that it is difficult to obtain the open channel current at high voltages ($|V| > 60$ mV) with increasing concentrations of SPD. On the contrary, enhancement of channel gating has been disregarded as the mechanism behind the effect of La^{3+} ions [36].

Next, we analyzed the full current-voltage relationships of OmpF at 100 mM KCl after the sequential addition of different concentrations of La, HexCo and SPD. Fig. 2A shows that increasing quantities of La decrease conductance mainly in positive voltages resulting in diode-like current-voltage curves [36,37]. In contrast, HexCo (Fig. 2B) and SPD (Fig. 2C) decrease channel conductance similarly at positive and negative applied voltages. The differential current reduction induced by the blockers has also varied effects on the channel current asymmetry. At the low salt concentration used here (100 mM KCl), the OmpF channel shows not completely Ohmic current-voltage (*I-V*) curves, but current is typically smaller at positive than at negative polarities [21]. This can be quantified by means of equation (1) used to characterize ideality of solid state diodes [53]. The parameter *n* is an ideality factor that usually ranges between 1 and 2 for semiconductor diodes. These are also the typical values for rectifying ion channels. For example, the channel-forming peptide Gramicidin A in asymmetrically charged bilayers showed a highly rectifying I-V curve yielding an $n \simeq 1.8$ [10]. For values of *n* high enough so that the exponential term in equation (1) can be linearized, the I-V curve becomes Ohmic. Fitting of control current-voltage curves (before addition of trivalent cations, black circles in Fig. 2A-C) with equation (1) yields $n \sim 19$, which

seems reasonable for a close-to-Ohmic system. Successive additions of La (Fig. 2A) increase the intrinsic current asymmetry, yielding an $n \sim 6$ for 15 mM La. This current asymmetry is mild compared to that obtained in OmpF using asymmetric pH and lipid composition [65–68] or in other systems [10,16,69–72]. Contrary to the effect of La, n increases appreciably after addition of 15 mM HexCo ($n \sim 50$, Fig. 2B) and orders of magnitude with 15 mM SPD ($n \sim 10^6$, Fig. 2C). This later value may be overestimated due to the lack of data in Fig. 2C for $|V| > 60$ mV. Still, the increase of n is clear. Therefore, La exaggerates OmpF intrinsic current asymmetry while HexCo and SPD cancel it, indicating the putative existence of different mechanisms of ion adsorption.
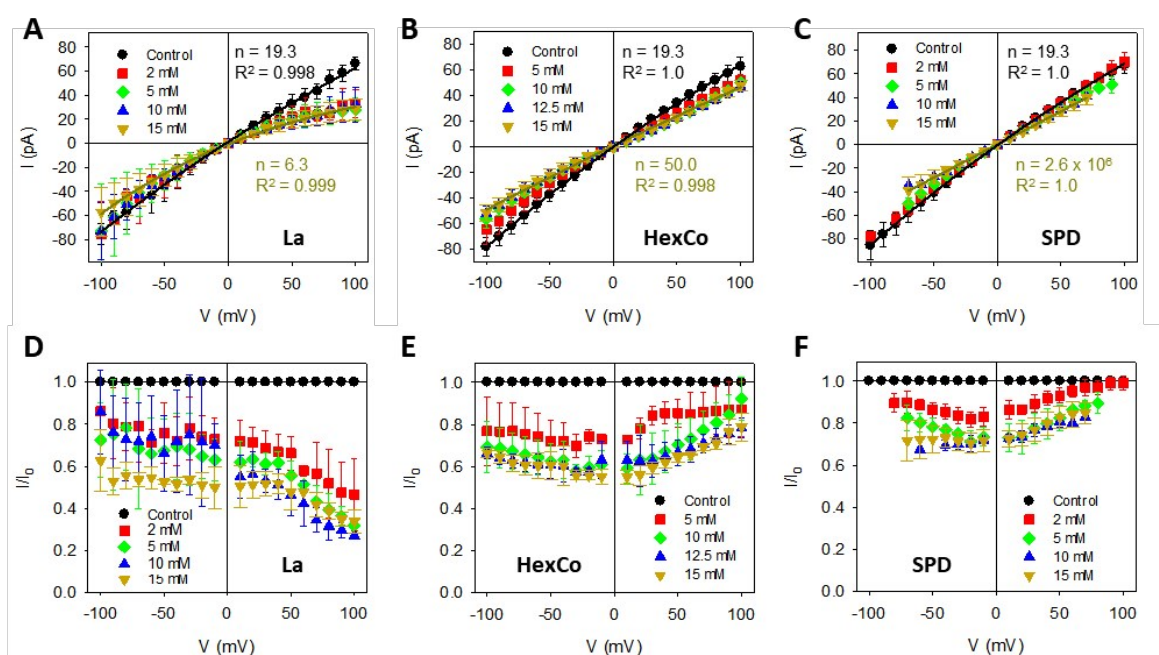

Figure 2. Symmetric addition of trivalent cations has a variable effect on OmpF single-channel current-voltage characteristics. (A-C) Single-channel current–voltage curves before and after the addition of increasing millimolar concentrations of La (A), HexCo (B), and SPD (C). Solid lines correspond to the fitting of experimental data to Equation (1). **(D-F)** Current rectification ratio I/I_0 induced by La (D), HexCo (E), and SPD (F) as a function of the applied voltage. I/I_0 is defined as the current with trivalent cations divided by the control current.

The diverse effect the trivalent cations on OmpF intrinsic current asymmetry indicates that the current is not decreased equally at both polarities. This is better observed using the so-called rectification ratio, calculated as the current at a given trivalent cation concentration over the control current, as shown in Figs. 2D-F. In the case of La (Fig. 2D), current rectification increases as voltage increases and the more concentrated the ion the higher rectification appears, so that values down to $I/I_0 \sim 0.3$ can be achieved with 15 mM La at +100 mV. In contrast, Figs. 2E,F show that HexCo and SPD effect is stronger at negative polarities and the current rectification is barely sensitive to the absolute voltage, with maximum values of $I/I_0 \sim 0.6$-0.7. Of note, a higher effect at negative than positive polarity explains the asymmetry reduction observed in Fig. 2B,C, given that control currents are higher at negative voltages.

Altogether, data in Fig. 2 demonstrates that La, HexCo and SPD induce different levels of current rectification in OmpF and enhance (La) or correct (HexCo, SPD) the channel intrinsic current asymmetry.

3.2. Noise analysis: equilibrium *vs* non-equilibrium fluctuations

The interactions between trivalent cations and OmpF porin are rather specific and yield pronounced differences in the conductive properties of the channel, as shown in Figs. 1 and 2. To gain new insights into the nature of these interactions we analyze the open channel noise and its dependence on frequency. The rationalization of PSD from membrane channels is usually very complex due to the presence of many different contributions, such as flicker and thermal noise, and capacitive or dielectric contributions [73]. Still, it is a useful tool used to uncover mechanisms of ion permeation in channels and nanopores. For example, previous noise studies in OmpF show PSDs with a characteristic Lorentzian-like shape [21,74]. Such noise pattern, especially evident at

high salt concentration (~ 1M KCl) [21] was attributed to the competitive binding of cations and

protons occurring in the narrow central constriction of the channel [75]. Fig. 3A shows representative

power spectra corresponding to current traces of OmpF in 100 mM KCl in the absence of any other

salts. Here, PSDs are far more complex than single lorentzians because the use of lower salt

concentration both weakens the competitive binding and increments the background noise.

Remarkably, PSDs recorded for positive (+50 mV) and negative (-50 mV) voltages are rather

similar and clearly separated from the background noise corresponding to the open channel at 0

mV. The effects of addition of millimolar concentrations of salts of trivalent cations are presented

in Fig. 3B, 3C, and 3D for La, HexCo, and SPD, respectively. We observe common features, like

the difference between background noise (PSD at 0 mV) and the PSD values at ± 50 mV is smaller

than in the control. However, significant differences are found as regards the polarity of the applied

voltage. While in control conditions (Fig 3A) both PSDs for positive and negative voltages show

similar levels of noise, PSDs after addition of La (Fig. 3B) show higher noise amplitudes at low

frequency for positive voltages than for negative. In contrast, addition of HexCo (Fig. 3C) yields

PSDs that resemble those of the control (without HexCo, Figure 3A): the noise levels are similar

for the two voltage polarities. Finally, in the case of SPD (Fig. 3D) the higher noise levels happen

for negative voltages. To better quantify these divergent effects, we calculated the normalized

noise, defined as the magnitude of the power spectrum at a chosen frequency (here we averaged

the low frequency region 2-20 Hz) divided by the squared value of the corresponding averaged

current, paying attention to its dependence on applied voltage, as shown in Fig. 3E. It has been

shown previously that conductance fluctuations depend on I^2 [55–61]. Therefore, a constant PSD/I^2

for changing voltages indicates that the current fluctuations recorded correspond to conductance

fluctuations of an equilibrium nature (see section 2.4 in Methods for more details). Control

measurements (black circles) and experiments incorporating trace amounts of HexCo (blue diamonds) show normalized PSDs that are almost voltage-independent pointing to equilibrium conductance fluctuations [57,59]. Quite in contrast, non-equilibrium features (normalized PSD increases with V) clearly appear in La (red triangles) for positive voltages and in SPD (green squares) for negative ones (note that high values of the normalized PSD at low voltages are due to very low values of the current that decrease the signal to noise ratio [60]).
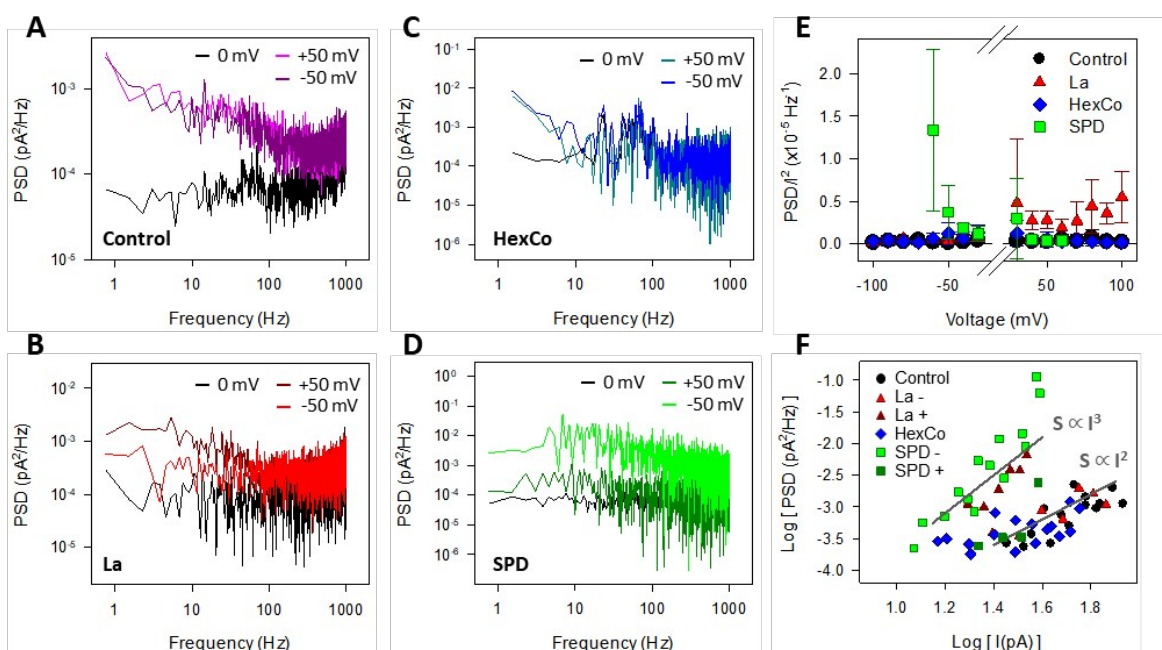

Figure 3. Millimolar concentrations of trivalent cations alter OmpF channel current fluctuations. **(A-D)** Representative power spectral densities (PSDs) of OmpF single channel current recorded at 0 and ±50 mV before (A) and after the symmetrical addition of 15 mM La (B), HexCo (C), and SPD (D). **(E)** Normalized PSDs (defined as the average magnitude of the power spectrum in the low frequency region 2-20 Hz divided by the squared value of the corresponding average current) as a function of the applied voltage before and after the symmetrical addition of 15 mM blocker. **(F)** Average PSD (over the low frequency region 2-20 Hz) as a function of the corresponding averaged current, in logarithmic values, for control conditions (black circles), 15 mM La at positive (dark red triangles) and negative (light red triangles) applied voltages, 15 mM HexCo (blue diamonds), and 15 mM SPD at positive (dark green squares) and negative (light green squares) applied voltages.

Equilibrium conductance fluctuations have been previously reported in single silicon nitride pores for both positive and negative voltages [59]. On the contrary, non-equilibrium fluctuations have been found for one or the two voltage polarities in polymeric [60,61,76] and solid-state rectifying nanopores [77]. In the latter ones, non-equilibrium noise was linked to trapping-detrapping processes that could induce transient fluctuations in the total number of ions when the trap becomes filled or unfilled [77]. Applying this model to solid-state conical nanopores, it was shown that normalized noise (PSD/$<I>^2$) is roughly proportional to the absolute current I [77], giving rise to an approximate scaling behavior of PSD α I^3, also found in other glass pores [76]. Interestingly, our measurements seem to follow similar patterns, as shown in Fig. 3F. Control measurements (black circles) and results with HexCo (blue diamonds) at any polarity, negative voltages in La (red triangles), and positive voltages in SPD (dark green squares) follow equilibrium S α I^2 scaling, whereas positive voltages in La (dark red triangles) and negative voltages in SPD (green squares) seem to follow the non-equilibrium scaling S α I^3 previously reported in Refs. [77] and [76].

3.3. Selectivity inversion

Since both equilibrium and non-equilibrium processes regulate ionic conductance in the presence of multivalent cations in trace amounts, we decided to explore how ion channel selectivity is affected. Considering that in some cases voltage polarity matters (current rectification, non-equilibrium fluctuations), we set as control conditions a ten-fold concentration gradient in both orientations, 1/0.1 M KCl and 0.1/1 M KCl, and added increasing amounts of salts of trivalent cations as shown in Fig. 4 for La (Fig. 4A), HexCo (Fig, 4B) and SPD (Fig. 4C). La (Fig. 4A) is the less effective one in turning the canonical cation selectivity of the channel [21,22] into anionic

one, almost by a factor of five (25 mM versus 5 mM) in comparison with HexCo (Fig. 4B), being

SPD (Fig. 4C) somewhere in the middle. In addition, La is the one showing more visible

differences between the two gradient orientations, while for HexCo values fall within the

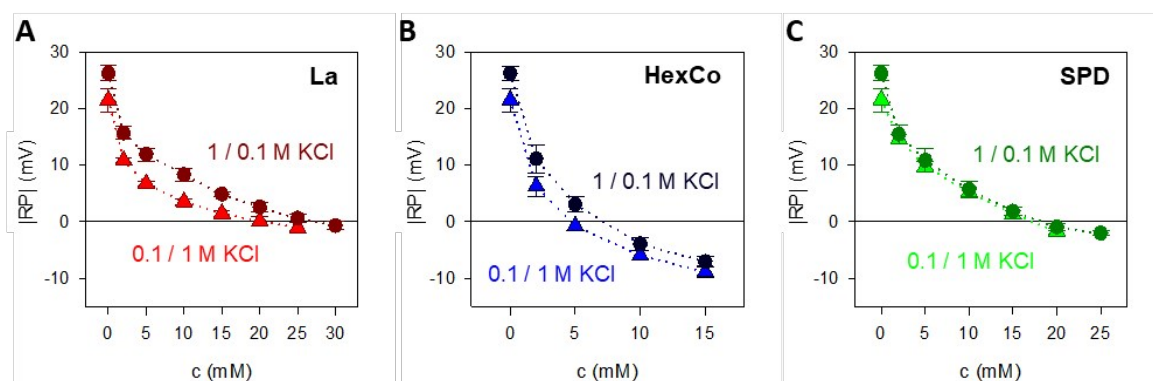experimental error and in SPD differences are inappreciable.

Figure 4. Millimolar concentrations of trivalent cations invert the OmpF cationic selectivity.
Absolute values of the reversal potential (RP) obtained from experiments in 1/0.1 M KCl (dark
colored circles) and 0.1/1 M KCl (light colored triangles) before and after the symmetrical addition
of increasing concentrations of La **(A)**, HexCo **(B)**, and SPD **(C)**.

Thus, millimolar concentrations of all tested trivalent electrolytes invert the measured selectivity,

which is generally ascribed to a channel charge inversion, as reported for OmpF and other

mesoscopic ion channels and nanopores in the presence of multivalent electrolytes [13,16,17,43,78]. The

OmpF channel charge is more effectively inverted by La, HexCo and SPD when *cis* is the side

with lower KCl concentration and the effect is stronger as hydrated radius decreases HexCo < SPD

< La [79–82]. The charge inversion seems to occur regardless of the existence (La, SPD) or not

(HexCo) of non-equilibrium fluctuations.

The effect of the concentration gradient direction and voltage polarity is more clearly seen in the

current-voltage characteristics. Fig. 5 shows representative *I-V* curves of OmpF under the

concentration gradient 1/0.1 M KCl (dark colors) and 0.1/1 M KCl (light colors), before (Fig. 5A)

and after the addition of 15 mM La, HexCo, or SPD (Fig. 5B-D). In control conditions (Fig. 5A),

the *I-V* curves are shifted from zero due to the OmpF cationic selectivity [21,22]. Symmetrical addition

of 15 mM La (Fig. 5B) has two complementary effects: on the one hand, it shifts back the reversal

potential towards zero (as shown in Fig. 4A). On the other hand, La induces a change in the current

compared to the corresponding control (Fig. 5A) that is stronger as voltage becomes more positive.

Thus, at negative voltages the curves are separated and agree with control values, while at positive

voltages they fall on top of each other with intermediate values between control measurements.

Interestingly, the positive polarity is the one showing non-equilibrium fluctuations (Fig. 3E).
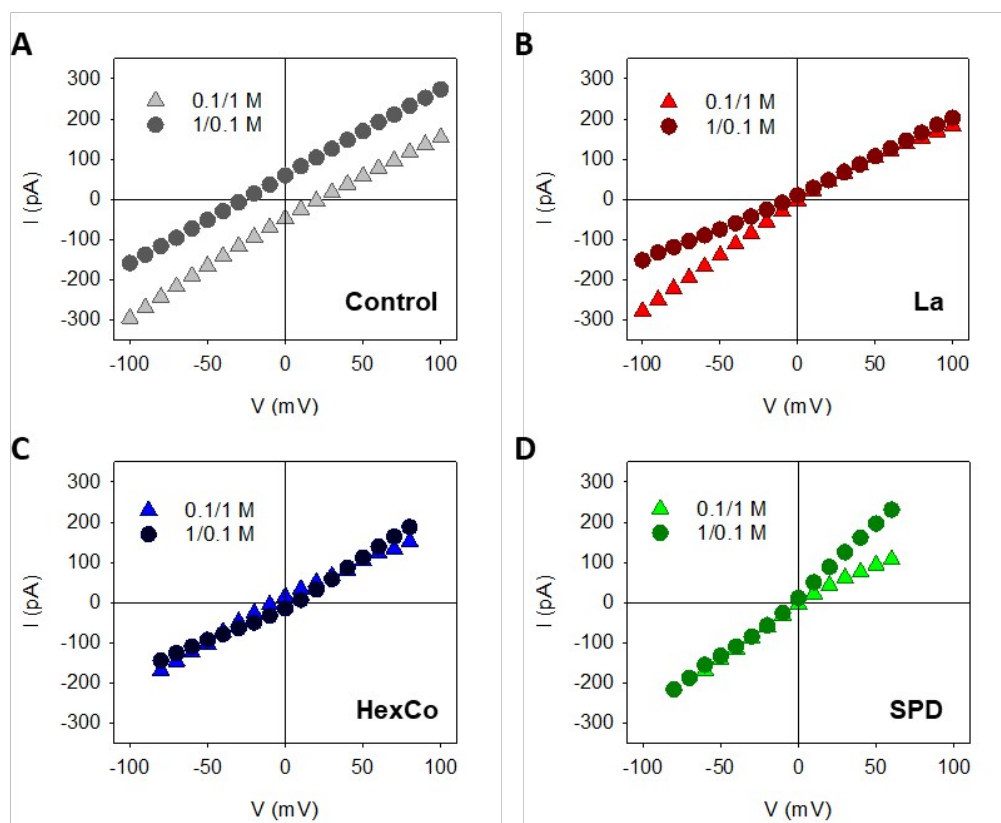

Figure 5. La, HexCo and SPD induce diverse effects in the OmpF current-voltage characteristics under concentration gradient. Representative single-channel *I-V* curves recorded

in KCl under a concentration gradient of 1/0.1 M (dark colored circles) and 0.1/1 M KCl (light colored triangles) before **(A)** and after the symmetrical addition of 15 mM La **(B)**, HexCo **(C)**, or SPD **(D)**.

Addition of HexCo (Fig. 5C) induces a shift of the *I-V* curves that is similar at the two voltage polarities. However, the effect of SPD addition (Fig. 5D) is stronger at negative voltages, where the data from the two gradient orientations collapse differing from the corresponding control data (Fig. 5A), in contrast to the positive polarity where data points show similar values to control ones. Remarkably, the negative polarity is once again the one showing non-equilibrium fluctuations (Fig. 3E).

Therefore, experiments under concentration gradient reveal complex adsorption dynamics in which the specific effects of trivalent cations on OmpF channel function can be classified as having an equilibrium (selectivity inversion that does not depend on voltage polarity and only mildly on concentration gradient direction) or non-equilibrium (voltage-asymmetric effect of La and SPD addition) origin.

3.4. Mechanisms of surface charge regulation

We have shown in previous sections that current-voltage relationships, noise analysis and ion selectivity provide complementary insights on the channel surface charge regulation exerted by trivalent cations. We consider especially though-provoking the finding of non-equilibrium fluctuations and its possible association with trapping dynamics. We speculate that this mechanism may be present in OmpF channel. In previous studies, it was shown that either divalent and trivalent ions interact strongly with certain acidic residues located in the central narrow constriction of the channel [12,13,75]. Nonetheless, the effect of trivalent cations with the channel was shown to be reversible [36]: a fast switch of voltage polarity was enough to interrupt the interaction

and recover the control conductance. Importantly, this reversibility was demonstrated for fast ratchets of up to 100 Hz. Hence, the interactions between trivalent cations and the OmpF nanopore might be described as trapping-detrapping processes with particular characteristic times depending on the residue-cation particular chemistry [77]. Within this picture, tight (high energy) cation trapping would be equivalent to an equilibrium chemically-based adsorption, as seems to be the case of HexCo showing almost voltage-independent features in Fig. 2B, Fig. 3B, and Fig. 5C, and an efficient selectivity inversion as shown in Fig. 4B. In contrast, looser (low energy) cation trapping would induce fluctuations in the total number of ions (visible as non-equilibrium fluctuations) as happens with La and SPD. In these cases, selectivity inversion would be less efficient because the system fluctuates between the "trivalent cation-adsorbed" filled-trap and the empty-trap configuration, as shown in Fig. 4A,C, and the channel would show voltage-dependent features, as observed in Fig. 2A, Fig. 3E and Fig. 5B,D. The physical reasons behind the observed features may be related to the pore geometry. OmpF has an hour-glass shape with a central narrow constriction (7 x 11 Å in diameter [83]), in which steric effects may play a role favoring smaller HexCo (7.9 Å hydrated diameter) [79] in relation to larger La (9.1 Å hydrated diameter) [79] . SPD – with a diameter of around 9 Å [80–82] – not only shows intermediate features between HexCo and La in relation to selectivity inversion, but it also does not induce current rectification like HexCo and shows non-equilibrium fluctuations like La.

4. Conclusions

In conclusion, we have provided experimental evidence that the interaction of trivalent electrolytes with biological nanopores can yield specific modulation of ion conduction and charge inversion. We have also demonstrated that surface charge regulation can induce non-equilibrium fluctuations

possibly due to the existence of ion-specific trapping-detrapping processes. Our insights are relevant for biological and electrochemical systems involving transport phenomena in charged surfaces under nanoscale confinement.

AUTHOR CONTRIBUTIONS

María Queralt-Martín: Conceptualization, Methodology, Investigation, Validation, Formal analysis, Writing - Original Draft, Visualization, Supervision, Project administration. **D. Aurora Perini:** Investigation, Writing - Review & Editing. **Antonio Alcaraz:** Conceptualization, Methodology, Formal analysis, Writing - Original Draft, Supervision, Project administration, Funding acquisition.

CONFLICTS OF INTEREST

There are no conflicts of interest to declare.

ACKNOWLEDGMENTS

REFERENCES

1   L. Bocquet and E. Charlaix, Nanofluidics, from bulk to interfaces., *Chem. Soc. Rev.*, 2010, **39**, 1073–95.

2   M. Fuest, K. K. Rangharajan, C. Boone, A. T. Conlisk and S. Prakash, Cation Dependent Surface Charge Regulation in Gated Nanofluidic Devices, *Anal. Chem.*, 2017, **89**, 1593–1601.

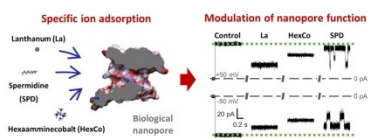3   P. Ramirez, J. A. Manzanares, J. Cervera, V. Gomez, M. Ali, S. Nasir, W. Ensinger and S.

Mafe, Surface charge regulation of functionalized conical nanopore conductance by divalent cations and anions, *Electrochim. Acta*, 2019, **325**, 134914.

4   B. Hille, *Ion Channels of Excitable Membranes*, Sinauer Associates Inc, Sunderland, MA, Third Ed., 2001, vol. Third Edit.

5   M. Queralt-Martín, M. L. López, M. Aguilella-Arzo, V. M. Aguilella and A. Alcaraz, Scaling Behavior of Ionic Transport in Membrane Nanochannels, *Nano Lett.*, 2018, **18**, acs.nanolett.8b03235.

6   F. H. J. Van Der Heyden, D. J. Bonthuis, D. Stein, C. Meyer and C. Dekker, Electrokinetic energy conversion efficiency in nanofluidic channels, *Nano Lett.*, 2006, **6**, 2232–2237.

7   J. Loessberg-Zahl, K. G. H. Janssen, C. McCallum, D. Gillespie and S. Pennathur, (Almost) Stationary Isotachophoretic Concentration Boundary in a Nanofluidic Channel Using Charge Inversion, *Anal. Chem.*, 2016, **88**, 6145–6150.

8   J. E. Dykstra, PhD Thesis, Wageningen University, 2018.

9   T. Luo, S. Abdu and M. Wessling, Selectivity of ion exchange membranes: A review, *J. Memb. Sci.*, 2018, **555**, 429–454.

10   P. a Gurnev and S. M. Bezrukov, Inversion of membrane surface charge by trivalent cations probed with a cation-selective channel., *Langmuir*, 2012, **28**, 15824–30.

11   O. Matsarskaia, F. Roosen-Runge and F. Schreiber, Multivalent ions and biomolecules: Attempting a comprehensive perspective, *ChemPhysChem*, 2020, 1–27.

12   A. Alcaraz, E. M. Nestorovich, M. L. López, E. García-Giménez, S. M. Bezrukov and V. M. Aguilella, Diffusion, exclusion, and specific binding in a large channel: a study of OmpF selectivity inversion., *Biophys. J.*, 2009, **96**, 56–66.

13   E. García-Giménez, A. Alcaraz and V. M. Aguilella, Overcharging below the nanoscale: Multivalent cations reverse the ion selectivity of a biological channel, *Phys. Rev. E*, 2010, **81**, 021912.

14   E. García-Giménez, M. L. López, V. M. Aguilella and A. Alcaraz, Linearity, saturation and blocking in a large multiionic channel: divalent cation modulation of the OmpF porin conductance., *Biochem. Biophys. Res. Commun.*, 2011, **404**, 330–4.

15   D. Gillespie, J. Giri and M. Fill, Reinterpreting the anomalous mole fraction effect: The ryanodine receptor case study, *Biophys. J.*, 2009, **97**, 2212–2221.

16   Y. He, D. Gillespie, D. Boda, I. Vlassiouk, R. S. Eisenberg and Z. S. Siwy, Tuning transport properties of nanofluidic devices with local charge inversion., *J. Am. Chem. Soc.*, 2009, **131**, 5194–202.

17   P. Ramirez, J. A. Manzanares, J. Cervera, V. Gomez, M. Ali, I. Pause, W. Ensinger and S. Mafe, Nanopore charge inversion and current-voltage curves in mixtures of asymmetric electrolytes, *J. Memb. Sci.*, 2018, **563**, 633–642.

18   S. Nasir, M. Ali, J. Cervera, V. Gomez, M. Hamza Ali Haider, W. Ensinger, S. Mafe and P. Ramirez, Ionic transport characteristics of negatively and positively charged conical nanopores in 1:1, 2:1, 3:1, 2:2, 1:2, and 1:3 electrolytes, *J. Colloid Interface Sci.*, 2019, **553**, 639–646.

19   H. Nikaido, Molecular Basis of Bacterial Outer Membrane Permeability Revisited, *Microbiol. Mol. Biol. Rev.*, 2003, **67**, 593–656.

20   A. H. Delcour, Solute uptake through general porins, *Front. Biosci.*, 2003, **8**, D1055–

Physical Chemistry Chemical Physics Accepted Manuscript

D1071.

21   E. M. Nestorovich, T. K. Rostovtseva and S. M. Bezrukov, Residue ionization and ion transport through OmpF channels, *Biophys. J.*, 2003, **85**, 3718–3729.

22   A. Alcaraz, E. M. Nestorovich, M. Aguilella-Arzo, V. M. Aguilella and S. M. Bezrukov, Salting out the ionic selectivity of a wide channel: the asymmetry of OmpF., *Biophys. J.*, 2004, **87**, 943–57.

23   M. L. López, M. Aguilella-Arzo, V. M. Aguilella and A. Alcaraz, Ion selectivity of a biological channel at high concentration ratio: insights on small ion diffusion and binding., *J. Phys. Chem. B*, 2009, **113**, 8745–51.

24   M. L. López, E. García-Giménez, V. M. Aguilella and A. Alcaraz, Critical assessment of OmpF channel selectivity: merging information from different experimental protocols., *J. Physics. Condens. Matter*, 2010, **22**, 454106.

25   W. Im and B. Roux, Ions and counterions in a biological channel: a molecular dynamics simulation of OmpF porin from Escherichia coli in an explicit membrane with 1 M KCl aqueous salt solution., *J. Mol. Biol.*, 2002, **319**, 1177–97.

26   W. Im and B. Roux, Ion permeation and selectivity of OmpF porin: a theoretical study based on molecular dynamics, Brownian dynamics, and continuum electrodiffusion theory, *J. Mol. Biol.*, 2002, **322**, 851–869.

27   A. Alcaraz, M. L. López, M. Queralt-Martín and V. M. Aguilella, Ion Transport in Confined Geometries below the Nanoscale: Access Resistance Dominates Protein Channel Conductance in Diluted Solutions, *ACS Nano*, 2017, **11**, 10392–10400.

28   J. C. T. Eijkel and A. van den Berg, Nanofluidics: what is it and what can we expect from it?, *Microfluid. Nanofluidics*, 2005, **1**, 249–267.

29   D. A. McCurry and R. C. Bailey, Electrolyte Gradient-Based Modulation of Molecular Transport through Nanoporous Gold Membranes., *Langmuir*, 2017, **33**, 1552–1562.

30   S. Howorka and Z. Siwy, Nanopore analytics: sensing of single molecules, *Chem. Soc. Rev.*, 2009, **38**, 2360.

31   B. M. Venkatesan and R. Bashir, Nanopore sensors for nucleic acid analysis, *Nat. Nanotechnol.*, 2011, **6**, 615–624.

32   F. Olasagasti, K. R. Lieberman, S. Benner, G. M. Cherf, J. M. Dahl, D. W. Deamer and M. Akeson, Replication of individual DNA molecules under electronic control using a protein nanopore, *Nat. Nanotechnol.*, 2010, **5**, 798–806.

33   K. Göpfrich, C.-Y. Li, I. Mames, S. P. Bhamidimarri, M. Ricci, J. Yoo, A. Mames, A. Ohmann, M. Winterhalter, E. Stulz, A. Aksimentiev and U. F. Keyser, Ion Channels Made from a Single Membrane-Spanning DNA Duplex, *Nano Lett.*, 2016, **16**, 4665–4669.

34   L. Movileanu, Watching Single Proteins Using Engineered Nanopores, *Protein Pept. Lett.*, 2014, **21**, 235–246.

35   H. Bajaj, S. Acosta Gutierrez, I. Bodrenko, G. Malloci, M. A. Scorciapino, M. Winterhalter and M. Ceccarelli, Bacterial Outer Membrane Porins as Electrostatic Nanosieves: Exploring Transport Rules of Small Polar Molecules, *ACS Nano*, 2017, **11**, 5465–5473.

36   C. Verdiá-Báguena, M. Queralt-Martín, V. M. Aguilella and A. Alcaraz, Protein Ion Channels as Molecular Ratchets. Switchable Current Modulation in Outer Membrane Protein F Porin Induced by Millimolar La 3+ Ions, *J. Phys. Chem. C*, 2012, **116**, 6537–

6542.

37   M. Queralt-Martín, C. Verdiá-Báguena, V. M. Aguilella and A. Alcaraz, Electrostatic Interactions Drive the Nonsteric Directional Block of OmpF Channel by La 3+, *Langmuir*, 2013, **29**, 15320–15327.

38   L. H. Wang, N. Jiang, B. Zhao, X. D. Li, T. H. Lu, X. L. Ding and X. H. Huang, Structural basis for the decrease in the outward potassium channel current induced by lanthanum., *J. Biol. Inorg. Chem.*, 2010, **15**, 989–93.

39   D. Fologea, E. Krueger, R. Al Faori, R. Lee, Y. I. Mazur, R. Henry, M. Arnold and G. J. Salamo, Multivalent ions control the transport through lysenin channels., *Biophys. Chem.*, 2010, **152**, 40–5.

40   M. C. Sanguinetti and N. K. Jurkiewicz, Lanthanum blocks a specific component of IK and screens membrane surface change in cardiac cells., *Am. J. Physiol.*, 1990, **259**, H1881-9.

41   H. Gögelein, H. de Smedt, W. van Driessche and R. Borghgraef, The effect of lanthanum on alamethicin channels in black lipid bilayers, *Biochim. Biophys. Acta - Biomembr.*, 1981, **640**, 185–194.

42   D. A. Hanck and M. F. Sheets, Extracellular divalent and trivalent cation effects on sodium current kinetics in single canine cardiac Purkinje cells., *J. Physiol.*, 1992, **454**, 267–298.

43   K. Lin, C. Y. Lin, J. W. Polster, Y. Chen and Z. S. Siwy, Charge Inversion and Calcium Gating in Mixtures of Ions in Nanopores, *J. Am. Chem. Soc.*, 2020, **142**, 2925–2934.

44   P. Ramirez, J. Cervera, M. Ali, S. Nasir, W. Ensinger and S. Mafe, Impact of Surface Charge Directionality on Membrane Potential in Multi-ionic Systems, *J. Phys. Chem. Lett.*, 2020, **11**, 2530–2534.

45   A. Gilardi, S. P. Bhamidimarri, M. Brönstrup, U. Bilitewski, R. K. R. Marreddy, K. M. Pos, L. Benier, P. Gribbon, M. Winterhalter and B. Windshügel, Biophysical characterization of E. coli TolC interaction with the known blocker hexaamminecobalt, *Biochim. Biophys. Acta - Gen. Subj.*, 2017, **1861**, 2702–2709.

46   A. L. Dela Vega and A. H. Delcour, Polyamines decrease Escherichia coli outer membrane permeability, *J. Bacteriol.*, 1996, **178**, 3715–3721.

47   T. Gamble, K. Decker, T. S. Plett, M. Pevarnik, J. F. Pietschmann, I. Vlassiouk, A. Aksimentiev and Z. S. Siwy, Rectification of ion current in nanopores depends on the type of monovalent cations: Experiments and modeling, *J. Phys. Chem. C*, 2014, **118**, 9809–9819.

48   M. Zorkot, R. Golestanian and D. J. Bonthuis, The Power Spectrum of Ionic Nanopore Currents: The Role of Ion Correlations, *Nano Lett.*, 2016, **16**, 2205–2212.

49   E. Largo, M. Queralt-Martín, P. Carravilla, J. L. Nieva and A. Alcaraz, Single-molecule conformational dynamics of viroporin ion channels regulated by lipid-protein interactions, *Bioelectrochemistry*, 2021, **137**, 107641.

50   S. M. Bezrukov and I. Vodyanoy, Probing alamethicin channels with water-soluble polymers. Effect on conductance of channel states., *Biophys. J.*, 1993, **64**, 16–25.

51   M. Montal and P. Mueller, Formation of bimolecular membranes from lipid monolayers and a study of their electrical properties., *Proc. Natl. Acad. Sci. U. S. A.*, 1972, **69**, 3561–6.

52   A. Alcaraz, P. Ramírez, E. García-Giménez, M. L. López, A. Andrio and V. M. Aguilella, A pH-tunable nanofluidic diode: electrochemical rectification in a reconstituted single ion

Physical Chemistry Chemical Physics Accepted Manuscript

channel., *J. Phys. Chem. B*, 2006, **110**, 21205–9.

53   A. Jain and A. Kapoor, A new method to determine the diode ideality factor of real solar cell using Lambert W-function, *Sol. Energy Mater. Sol. Cells*, 2005, **85**, 391–396.

54   L. J. DeFelice, *Introduction to Membrane Noise*, Springer US, Boston, MA, 1981.

55   C. Tasserit, A. Koutsioubas, D. Lairez, G. Zalczer and M.-C. Clochard, Pink noise of ionic conductance through single artificial nanopores revisited., *Phys. Rev. Lett.*, 2010, **105**, 260602.

56   E. Rigo, Z. Dong, J. H. Park, E. Kennedy, M. Hokmabadi, L. Almonte-Garcia, L. Ding, N. Aluru and G. Timp, Measurements of the size and correlations between ions using an electrolytic point contact, *Nat. Commun.*, 2019, **10**, 2382.

57   S. M. Bezrukov and M. Winterhalter, Examining Noise Sources at the Single-Molecule Level: 1/f Noise of an Open Maltoporin Channel, *Phys. Rev. Lett.*, 2000, **85**, 202–205.

58   S. M. Bezrukov and I. Vodyanoy, in *Biomembrane Electrochemistry*, eds. M. B. Blank and I. Vodyanoy, 1994, pp. 375–399.

59   D. P. Hoogerheide, S. Garaj and J. A. Golovchenko, Probing surface charge fluctuations with solid-state nanopores, *Phys. Rev. Lett.*, 2009, **102**, 256804.

60   M. R. Powell, I. Vlassiouk, C. Martens and Z. S. Siwy, Nonequilibrium 1/f noise in rectifying nanopores., *Phys. Rev. Lett.*, 2009, **103**, 248104.

61   M. R. Powell, N. Sa, M. Davenport, K. Healy, I. Vlassiouk, S. E. Létant, L. A. Baker and Z. S. Siwy, Noise properties of rectifying nanopores, *J. Phys. Chem. C*, 2011, **115**, 8775–8783.

62   D. A. Perini, A. Alcaraz and M. Queralt-Martín, Lipid Headgroup Charge and Acyl Chain Composition Modulate Closure of Bacterial β-Barrel Channels, *Int. J. Mol. Sci.*, 2019, **20**, 674.

63   R. Iyer and A. H. Delcour, Complex inhibition of OmpF and OmpC bacterial porins by polyamines, *J. Biol. Chem.*, 1997, **272**, 18595–18601.

64   E. M. Nestorovich and S. M. Bezrukov, in *Proc. SPIE 5467, Fluctuations and Noise in Biological, Biophysical, and Biomedical Systems II*, eds. D. Abbott, S. M. Bezrukov, A. Der and A. Sanchez, 2004, p. 42.

65   E. García-Giménez, A. Alcaraz, V. M. Aguilella and P. Ramírez, Directional ion selectivity in a biological nanopore with bipolar structure, *J. Memb. Sci.*, 2009, **331**, 137–142.

66   M. L. López, M. Queralt-Martín and A. Alcaraz, Stochastic pumping of ions based on colored noise in bacterial channels under acidic stress, *Nanoscale*, 2016, **8**, 13422–13428.

67   M. Queralt-Martín, C. Peiró-González, M. Aguilella-Arzo and A. Alcaraz, Effects of extreme pH on ionic transport through protein nanopores: the role of ion diffusion and charge exclusion, *Phys. Chem. Chem. Phys.*, 2016, **18**, 21668–21675.

68   M. Queralt-Martín, E. García-Giménez, V. M. Aguilella, P. Ramirez, S. Mafe and A. Alcaraz, Electrical pumping of potassium ions against an external concentration gradient in a biological ion channel, *Appl. Phys. Lett.*, 2013, **103**, 043707.

69   M. Ali, I. Ahmed, S. Nasir, P. Ramirez, C. M. Niemeyer, S. Mafe and W. Ensinger, Ionic Transport through Chemically Functionalized Hydrogen Peroxide-Sensitive Asymmetric Nanopores, *ACS Appl. Mater. Interfaces*, 2015, **7**, 19541–19545.

70   M. Ali, S. Nasir, P. Ramirez, J. Cervera, S. Mafe and W. Ensinger, Calcium binding and

ionic conduction in single conical nanopores with polyacid chains: model and experiments., *ACS Nano*, 2012, **6**, 9247–57.

71   Z. S. Siwy and A. Fuliński, A nanodevice for rectification and pumping ions, *Am. J. Phys.*, 2004, **72**, 567.

72   G. Maglia, A. J. Heron, W. L. Hwang, M. A. Holden, E. Mikhailova, Q. Li, S. Cheley and H. Bayley, Droplet networks with incorporated protein diodes show collective properties., *Nat. Nanotechnol.*, 2009, **4**, 437–40.

73   C. Wen, S. Zeng, K. Arstila, T. Sajavaara, Y. Zhu, Z. Zhang and S. L. Zhang, Generalized Noise Study of Solid-State Nanopores at Low Frequencies, *ACS Sensors*, 2017, **2**, 300–307.

74   M. Queralt-Martín, M. L. L. López and A. Alcaraz, Excess white noise to probe transport mechanisms in a membrane channel, *Phys. Rev. E*, 2015, **91**, 062704.

75   A. Alcaraz, M. Queralt-Martín, E. García-Giménez and V. M. Aguilella, Increased salt concentration promotes competitive block of OmpF channel by protons, *Biochim. Biophys. Acta - Biomembr.*, 2012, **1818**, 2777–2782.

76   S. F. Knowles, U. F. Keyser and A. L. Thorneywork, Noise properties of rectifying and non-rectifying nanopores, *Nanotechnology*, 2020, **31**, 10LT01.

77   S. Su, X. Guo, Y. Fu, Y. Xie, X. Wang and J. Xue, Origin of nonequilibrium 1/: F noise in solid-state nanopores, *Nanoscale*, 2020, **12**, 8975–8981.

78   S. Buyukdagli and T. Ala-Nissila, Controlling polymer translocation and ion transport via charge correlations, *Langmuir*, 2014, **30**, 12907–12915.

79   E. R. Nightingale, Phenomenological Theory of Ion Solvation. Effective Radii of Hydrated Ions, *J. Phys. Chem.*, 1959, **63**, 1381–1387.

80   Database indicating the size of spermidine, http://www.3dmet.dna.affrc.go.jp/cgi/show_data.php?acc=B01214, (accessed 24 August 2020).

81   H. Ohishi, I. Nakanishi, K. Inubushi, G. Van Der Marel, J. H. Van Boom, A. Rich, A. H. J. Wang, T. Hakoshima and K. I. Tomita, Interaction between the left-handed Z-DNA and polyamine-2: The crystal structure of the d(CG)3 and spermidine complex, *FEBS Lett.*, 1996, **391**, 153–156.

82   R. Zhang and B. I. Shklovskii, The pulling force of a single DNA molecule condensed by spermidine, *Phys. A Stat. Mech. its Appl.*, 2005, **349**, 563–570.

83   S. W. Cowan, T. Schirmer, G. Rummel, M. Steiert, R. Ghosh, R. A. Pauptit, J. N. Jansonius and J. P. Rosenbusch, Crystal structures explain functional properties of two E. coli porins., *Nature*, 1992, **358**, 727–33.

190x254mm (300 x 300 DPI)